A Decomposition of the Key Drivers of Current and Future Northern Hemisphere Cyclone-Associated Precipitation Trends

ALEX CRAWFORD [a,b] MICHELLE MCCRYSTALL,[c] AND NICOLE LOEB[a]

[a] *Department of Environment and Geography, University of Manitoba, Winnipeg, Manitoba, Canada*
[b] *Centre for Earth Observation Science, University of Manitoba, Winnipeg, Manitoba, Canada*
[c] *Department of Physics, University of Auckland, Auckland, New Zealand*

ABSTRACT: Extratropical cyclones are responsible for most precipitation falling north of 40°N, especially in winter. Greater moisture availability in a warmer world is expected to boost the intensity of cyclone-associated precipitation (CAP), but how changes in cyclone frequency and intensity impact this trend is uncertain. Here, we use two atmospheric reanalyses and 18 climate models participating in phase 6 of the Coupled Model Intercomparison Project (CMIP6) to update projections of future CAP. Models project that nearly the entire Northern Hemisphere exhibits increasing winter CAP with continued warming [by at least 5% $(1°C)^{-1}$ global warming throughout, and over 30% in the Arctic and eastern Asia]. Summer CAP increases over the Pacific Ocean (2%–10%) and Arctic (up to 20%) but decreases over midlatitude continents and the Atlantic Ocean (exceeding 20% in places). These outcomes result from the relative balance between two overarching and often opposing trends: Extratropical cyclones (and therefore CAP events) become less frequent (except in the Arctic), but the average event produces more precipitation in the future (especially by more intense precipitation rates). Historically, CAP intensity trends are driven more by moisture availability than cyclone intensity (i.e., stronger winds); projections indicate future CAP intensity enhancement will be driven almost entirely by moisture availability. The strongest CAP trends historically are increases on the west side of the midlatitude oceanic storm tracks, but projections indicate that the Arctic Ocean will exhibit the strongest positive future trends because of exceptional increases in moisture availability combined with little change to storm frequency or intensity.

SIGNIFICANCE STATEMENT: Large storms called extratropical cyclones are responsible for most precipitation falling in the midlatitudes and the Arctic, especially in winter. We examined 18 state-of-the-art climate models to update projections of how precipitation associated with these storms is likely to change with continued global warming. Overall, two dominant trends were that there are fewer storms in the future and that typical storms produce more precipitation in the future than today. These trends counteract each other. In winter, the trend toward more intense precipitation wins out, so storm-associated precipitation increases nearly everywhere. Notably, increased precipitation intensity is not related to the strength of the storms. Instead, the increase occurs almost entirely because of greater evaporation as the world warms.

1. Introduction

The intensification of the water cycle is a well-known atmospheric response to modern global warming (Bengtsson et al. 2011; O'Gorman et al. 2012; McCrystall et al. 2021; Allan et al. 2022). The Clausius–Clapeyron relationship shows a 7% increase in atmospheric water-holding capacity per degree of warming (Trenberth et al. 2003; Liu and Allan 2013), leading to an intensification of the hydrological cycle. This intensification comprises

ⓐ Denotes content that is immediately available upon publication as open access.

🖉 Supplemental information related to this paper is available at the Journals Online website: https://doi.org/10.1175/JCLI-D-24-0453.s1.

Corresponding author: Alex Crawford, alex.crawford@umanitoba.ca

enhanced evaporation, especially in the subtropics (Wentz et al. 2007; Liu and Allan 2013), greater poleward moisture transport (Held and Soden 2006; Rinke et al. 2019), and greater precipitation, including in the Arctic (Rawlins et al. 2010; Liu and Allan 2013). However, radiative cooling at the top of the atmosphere provides an energetic constraint on condensation, and therefore precipitation trends (Pendergrass and Hartmann 2014; Pithan and Jung 2021). Consequently, global precipitation does not increase as rapidly as the atmosphere's water-holding capacity (Allan et al. 2022), especially in model simulations (Wentz et al. 2007; Lorenz et al. 2010; O'Gorman and Muller 2010).

For the mid- and high latitudes, the role of extratropical cyclones is essential to understanding any observed or projected precipitation trend (Villamil-Otero et al. 2018; Naakka et al. 2019; Fearon et al. 2021). Indeed, precipitation associated with extratropical cyclones [hereafter "cyclone-associated precipitation (CAP)"] accounts for over 80% of the precipitation in the North Pacific and North Atlantic storm tracks (Hawcroft et al. 2012) and 74% of the annual poleward moisture flux at 70°N (Fearon et al. 2021).

Most studies of CAP trends have identified an increase in CAP in response to global warming, in line with the overall intensification of the water cycle (Finnis et al. 2007; Crawford and Serreze 2017; Yettella and Kay 2017). They also sometimes decompose such trends into "thermodynamic changes" (related to the Clausius–Clapeyron relationship) and "dynamic changes" (related to changes in cyclone frequency or intensity). Dynamic changes may reinforce, counteract, or even overwhelm thermodynamic changes. Finnis et al. (2007) found that the thermodynamic increase in Northern Hemisphere CAP in a future simulation by the Community Climate System Model was partially offset by a decline in cyclone frequency. Later studies with the Community Earth System Model Large Ensemble found that, in strong warming scenarios, thermodynamic factors dominate dynamic ones in driving simulated precipitation trends throughout the Arctic and the Icelandic low region (Crawford and Serreze 2017; Yettella and Kay 2017). By contrast, Oh et al. (2020) found dynamic factors to be dominant in forcing CAP trends in both a set of models from phase 5 of the Coupled Model Intercomparison Project (CMIP5) and in dynamically downscaled projections from version 2 of the Canadian Earth System Model. Their projections showed increasing winter CAP around the Aleutian low associated with increased storm frequency and intensity and decreasing winter CAP around the Icelandic low associated with decreased storm frequency and intensity. Similarly, Stroeve et al. (2011) attributed a 10-yr increase in autumn Arctic CAP in the early 2000s to more frequent and intense storms. Reconciling these opposing conclusions may require a more detailed decomposition of the drivers of CAP. Additionally, since most prior work has used the same family of models, addressing the same questions with the larger (and newer) set of CMIP6 climate models may also improve confidence in projections.

In this study, we advance our understanding of the future of CAP in three ways. First, we employ an ensemble of 18 climate models participating in CMIP6, which have shown improved ability to simulate Northern Hemisphere cyclones compared to prior modeling efforts (Harvey et al. 2020; Priestley et al. 2020; Song et al. 2021). Second, we evaluate the consistency of trends between historical observations (from an atmospheric reanalysis) and the CMIP6 projections. Third, we decompose historical trends and future projections of CAP in more detail than previous work, assessing the relative importance of CAP intensity, event frequency, and average event duration. Trends in CAP intensity are further decomposed into trends in moisture availability and cyclone intensity, and trends in total CAP hours are further decomposed into trends in cyclone hours and CAP probability (the ratio of hours with CAP to hours of cyclone activity). These decompositions provide deeper insight into the relative importance of the various factors driving CAP changes.

Using these advancements, we address the following research questions:

1) How has CAP changed in the recent past (1979–2021), and how will it change under future warming?

2) What are the contributions to this trend from CAP intensity, frequency, and duration?

3) What are the contributions to trends in CAP by thermodynamic and dynamic factors?

2. Data

a. ERA5 and MERRA-2

ERA5 is the fifth major global reanalysis produced by the European Centre for Medium-Range Weather Forecasts (Hersbach et al. 2018, 2020) and has been used extensively to study the climatology of extratropical cyclones (e.g., Rohrer et al. 2020; Vessey et al. 2020; Hu et al. 2023), the global water cycle (e.g., Allan et al. 2022; Sun et al. 2022), and interactions between them (Papritz et al. 2021; Crawford et al. 2022; Serreze et al. 2022). Downloaded fields have an hourly temporal resolution and $0.25° \times 0.25°$ spatial resolution. Sea level pressure is used for cyclone detection. The sea level pressure gradient and zonal and meridional winds at 850 hPa are used for cyclone intensity. Total and large-scale precipitation are used for the CAP analysis. Trends focus on the recent past (1979–2021).

Although modern reanalyses show good consistency in Northern Hemisphere extratropical cyclone trends since 1979 (Vessey et al. 2020), precipitation trends vary (C. Li et al. 2021). To ensure that observational CAP trends are robust, we repeat all observational analyses with the Modern-Era Retrospective Analysis for Research and Applications, version 2 (MERRA-2; Gelaro et al. 2017). In a comparison of five reanalyses, ERA5 and MERRA-2 were the best match to the observational Global Precipitation Climatology Project monthly analyses (C. Li et al. 2021). ERA5 is used as the primary data source here because (i) differences with MERRA-2 are relatively minor and (ii) ERA5 slightly outperforms other reanalyses at matching in situ observations of precipitation at high latitudes (Barrett et al. 2020; Loeb et al. 2022), although MERRA-2 is better in the subtropics (C. Li et al. 2021).

b. CMIP6

For making projections of future CAP, we used the historical and shared socioeconomic pathway (SSP5–8.5) experiments from CMIP6. "SSP5–8.5" stands for a "shared socioeconomic pathway," in which radiative forcing relative to the preindustrial climate is about 8.5 W m^{-2} by 2100. This experiment provides the broadest array of global annual temperature anomalies and the most available models of all SSPs. Sea level pressure ("psl") was available every 6 h for both experiments in 18 climate models (Table S1 in the online supplemental material). Cumulative total ("tp") and large-scale ("lsp") precipitation were available every 3 h for 13 models and every 24 h for the other five. For calculating global annual temperature anomalies, the monthly surface air temperature ("tas") was also acquired. Although models with higher spatial resolution have been shown to yield regional cyclone characteristics that better match atmospheric reanalyses (Song et al. 2021; Crawford et al. 2023), our results did not prove sensitive to spatial resolution for CAP trends. Therefore, we present a simple multimodel mean derived from a single run ("r1") of each model in sections 4 and 5. Note that

all following methods are applied separately to each model prior to calculating the multimodel mean, which is always the last processing step.

3. Methods

a. Cyclone detection and tracking

Synoptic-scale cyclones are identified and described using the Centre for Earth Observation Science (CEOS)/NSIDC extratropical cyclone tracking algorithm (Crawford et al. 2021), which detects extratropical cyclones as local minima in sea level pressure (i.e., grid cells must be lower pressure than all other cells within 200 km) on a pole-centered Lambert's azimuthal equal-area grid. Cyclone detection is conducted at 3-h temporal resolution and 25-km spatial resolution in ERA5, a 3-h $(100 \text{ km})^{-1}$ in MERRA-2, and a 6-h $(100 \text{ km})^{-1}$ resolution for CMIP6. Only minima for which the average pressure difference between the low pressure center and the ring of grid cells 900–1000 km away is at least 7.5 hPa are kept as "cyclone centers." Elevations over 1500 m are masked, and cyclone area is initially defined as the highest isobar for which no sea level pressure maxima and just a single cyclone center is enclosed. Next, cyclone centers are combined as multicenter systems if (i) they lie within 1200 km of each other and (ii) combining them would at least double the area enclosed (relative to the larger cyclone).

For tracking a cyclone center between two times (e.g., t_1 and t_2), a predicted location ($\hat{x}_2$) is calculated based on past propagation when available (if not, $\hat{x}_2 = x_1$). The cyclone center from t_2 that is closest to $\hat{x}_2$ is considered a continuation of the given track with one caveat: Cyclone centers are not permitted to travel faster than 150 km h^{-1}. If no cyclone center from t_2 is within 150 km h^{-1} of x_1, cyclolysis occurs. Only cyclones that meet the following criteria are considered for further analysis:

1) Lifespan is at least 24 h.
2) Track length is at least 1000 km.
3) The cyclone is observed at an elevation less than 500 m at least once.
4) The cyclone is observed at least 500 km away from its genesis point at least once.

These criteria remove spurious systems that arise from artifacts around areas of complex topography and stationary heat lows.

b. CAP

CAP is calculated following Crawford and Serreze (2017). First, for each 3-h or 6-h period, contiguous areas for which large-scale precipitation exceeds a rate of 1.5 mm day^{-1} are identified. If the temporal resolution is finer for the precipitation data, then the precipitation is summed so that the instantaneous cyclone observations lie at the middle of the precipitation summation period (e.g., for some CMIP6 models, 3-h precipitation totals ending at 1200 and 1500 UTC are both assigned to 6-h cyclone data at 1200 UTC). For the CMIP6 models with daily precipitation data, the precipitation rate is assumed to be constant for the entire day. Second, the total precipitation (including large-scale and convective) from a precipitation area is assigned to a cyclone if either (i) the precipitation area intersects the cyclone area or (ii) the nearest part of the precipitation area lies within 250 km of the cyclone center. Third, if one precipitation area is associated with multiple cyclones, the precipitation area is partitioned, with each grid cell assigned to the nearest cyclone center.

c. Decomposition of CAP trend

The sum of CAP (mm) received by a grid cell over the course of any period is equal to the product of the average CAP intensity (R; mm h^{-1}), the number of CAP events (N; events), and the average event duration [D; h (event)$^{-1}$] [Eq. (1)]:

$$\text{CAP} = R \times N \times D. \tag{1}$$

Total CAP in some future period (CAP_F) can be described as total CAP in the present period (CAP_P) plus the difference in CAP between the two periods (ΔCAP). Likewise, the relative importance of a change in a component variable to a change in CAP between a present P and future F period can be estimated by decomposing the future value of each component into the present value plus some change. Altogether, this yields the following equation:

$$\text{CAP}_F = \text{CAP}_P + \Delta\text{CAP} = (R_P + \Delta R)$$
$$\times (N_P + \Delta N) \times (D_P + \Delta D). \tag{2}$$

The expansion of Eq. (2) comprises eight terms, including the present CAP value (CAP_P), and four interaction terms. Because the interaction terms together comprise only a small fraction of the overall change in CAP, they are collected into a single "error" term E, and the total change in CAP is decomposed as

$$\text{CAP}_F - \text{CAP}_P = \Delta\text{CAP} = N_P D_P \Delta R$$
$$+ R_P D_P \Delta N + R_P N_P \Delta D + E. \tag{3}$$

For ERA5 trend decompositions, the change for each variable (e.g., R) is determined by calculating a linear trend (e.g., β_R^t) for 1979–2021 and multiplying by $\Delta t = 10$ years to represent a change over one decade, for example:

$$\Delta R = \Delta t \beta_R^t. \tag{4}$$

Relative differences are calculated in reference to average CAP 1979–2021, so, for example, a relative impact of a change in CAP intensity ΔR_* to CAP is reported as

$$\Delta R^* = \frac{N_P D_P \Delta R}{\text{CAP}_P} \times 100\%. \tag{5}$$

For each CMIP6 model (i), the linear trend of each variable (e.g., $\beta_{R,i}^T$) is calculated by regressing that variable (e.g., R_i) against the global annual surface air temperature anomaly (T_i'), with respect to 1850–1900 for all temperature anomalies

in the historical or SSP5–8.5 experiments from 1979 to 2099. For example, the multimodel mean of ΔR represents the average change in CAP intensity exhibited by models for ΔT change in global temperature:

$$\Delta R = \frac{\sum_i^n \Delta T \beta_{R,i}^T}{n}, \tag{6}$$

where $n = 18$, the number of model simulations. The baseline for relative differences is 1979–2014 (limited by the historical experiment), and the interval of change ΔT is 1°C. As in ERA5, differences are reported relative to the average baseline CAP.

d. Decomposition of CAP intensity trends

Similar to how a trend in CAP can be decomposed into trends in average intensity, event frequency, and average duration, the trend in average CAP intensity (R; mm h^{-1}) can be decomposed into a thermodynamic component (moisture availability trend) and a dynamic component (cyclone intensity trend) (Emori and Brown 2005; Yettella and Kay 2017). With only two components, it is also more feasible to include explicit consideration of the single interaction term. Following Yettella and Kay (2017), we accomplish this in a three-step process. First, for each 3-month period, we build a probability density function of storm intensity by sorting each cyclone observation into bins of 850-hPa wind speed (V; averaged within 1200 km of the cyclone center) with an interval of 1 m s^{-1} from $V < 7$ to $V > 18$ m s^{-1}. Second, we calculate the total precipitation that falls within a grid cell for a given 3-month period for each possible storm intensity bin. Unlike the prior analysis, this only includes "core" cyclone precipitation—that falling within a radius of 1200 km from a cyclone center, which omits some frontal precipitation falling far from a cyclone center, which is less likely to be controlled by wind speed and convergence in the cyclone core. Also, note that because a single value for precipitation and wind is taken for each storm observation, the data are essentially being smoothed. We use a smaller radius than Yettella and Kay (2017) because we are working with 3- and 6-h cyclone locations instead of daily. Third, change in CAP intensity between two periods can be described by

$$R_F - R_P = \sum_i [R_{Pi}(N_{Fi} - N_{Pi})] + \sum_i [(R_{Fi} - R_{Pi})N_{Pi}]$$
$$+ \sum_i [(R_{Fi} - R_{Pi}) \times (N_{Fi} - N_{Pi})], \tag{7}$$

where N_P and N_F are the relative frequency of each storm intensity bin (i) in the present and future periods, respectively, and R_{Pi} and R_{Fi} are the average precipitation rates for each storm intensity bin in each period. {Here, "future" is calculated as the average plus the trend over 10 years for ERA5 [as in Eq. (4)] or the trend over 1°C of warming for CMIP6 [as in Eq. (6)].} The first term describes changes in CAP intensity due to changes in the probability density function of cyclone

intensity (i.e., dynamic change). The second term describes changes in CAP intensity while holding the probability density function of storm intensity constant (i.e., thermodynamic change). The final term is the interaction. To test sensitivity to the choice of cyclone intensity metric, we repeated this analysis using the average pressure gradient within 1000 km of the cyclone center instead of 850-hPa wind speed.

e. Decomposition of trends in total CAP hours

Assigning a dynamic and thermodynamic component to trends in CAP event frequency N is less straightforward, but one useful decomposition is to compare the total hours with cyclone influence ("cyclone hours," C), and the total number of CAP hours [events × hours (event)$^{-1}$, or $N \times D$]. By definition, CAP cannot exist without a cyclone, so $C > N \times D$ and CAP hours can be decomposed into cyclone hours C and the ratio of CAP hours to cyclone hours (k; i.e., the probability that an hour with cyclone influence includes active precipitation):

$$k = \frac{N \times D}{C} \rightarrow N \times D = C \times k. \tag{8}$$

The "CAP probability" k depends on many things, such as the moisture content in the cyclone, the size of precipitation areas associated with the storm, and the efficiency of the storm at converting moisture into precipitation. Complicating any analysis, some of the same processes that impact CAP intensity also impact the presence or absence of CAP (e.g., a more intense storm may exhibit both heavier and more prolonged CAP). Therefore, the implications of a change in k are uncertain, but a significant change in C indicates that a change in cyclone hours (a dynamic factor) contributes to a change in CAP hours.

Since for any instantaneous field, C is a binary value (cyclone present or absent), we cannot build probability density functions like Eq. (7). However, we can still build a decomposition like Eq. (2):

$$\Delta(N \times D) = (C_F k_F) - (C_P k_P) = k_P \Delta C + C_P \Delta k + \Delta C \Delta k. \tag{9}$$

Variables ΔC, Δk, and $\Delta(N \times D)$ are calculated using Eq. (4) (for ERA5) or Eq. (6) (for CMIP6). The final term is the interaction term, which has a negligible contribution.

4. Historical trends in CAP

a. Overall CAP trends

Long-term trends in CAP are distinguishable in several regions (Fig. 1). From 1979 to 2021, winter CAP increased throughout eastern North America and on the western end of the Atlantic and Pacific storm tracks, with magnitudes up to 10% (decade)$^{-1}$ (Fig. 1a). The highest increase [over 10% (decade)$^{-1}$] occurred north of Svalbard. By decomposing the CAP trend into its several components (section 3c), we find that these regions also experienced an increase in CAP intensity (Fig. 1c). In some areas (such as around Japan), increasing CAP intensity led to a 6%–10% (decade)$^{-1}$ increase in
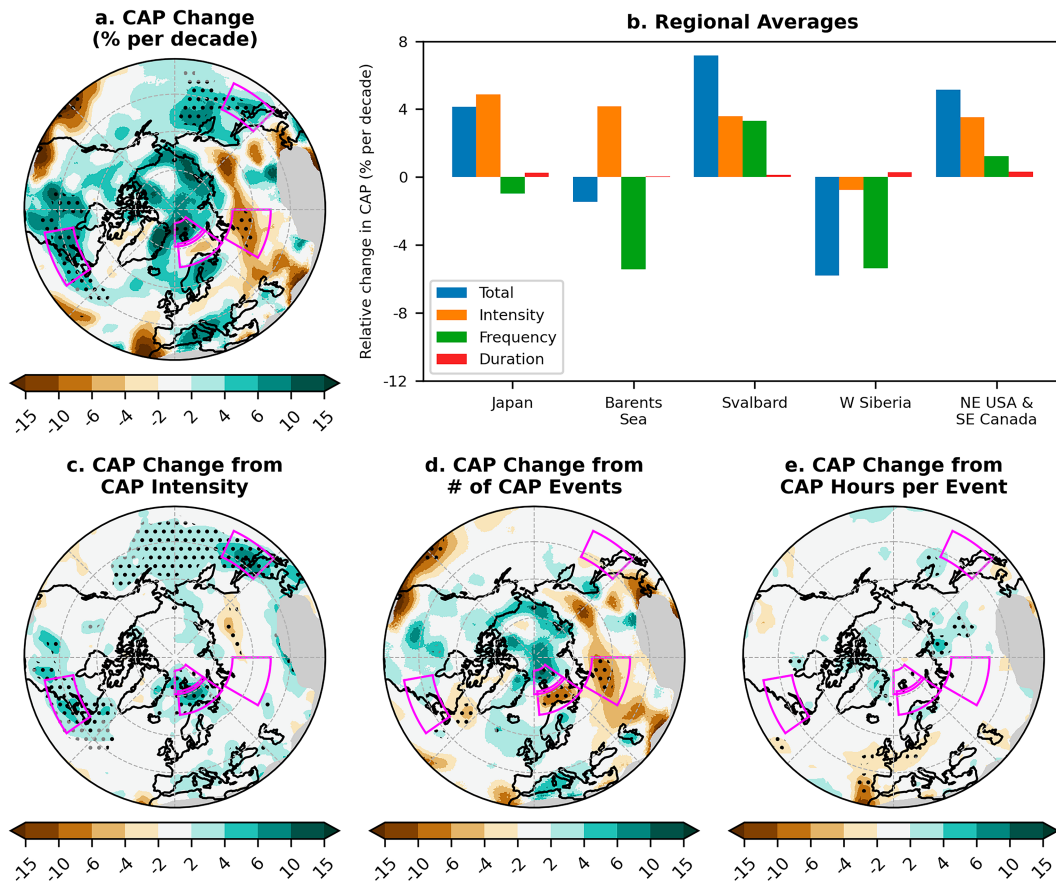
FIG. 1. (a) Relative change in total CAP [% (decade)$^{-1}$] during winter (DJF) based on ERA5 (1979–2021), and decomposition of that response into four factors: (c) intensity of precipitation during CAP events, (d) frequency of CAP events, and (e) the average duration of CAP events. All units are percent change in CAP per decade. Stippling indicates a significant trend ($p < 0.05$), with black (gray) stipples showing where MERRA-2 trends have the same (opposite) sign. (b) Regional averages of relative trend and its components for five illustrative areas (outlined in magenta). Minor error term not shown.

total CAP, which accounts for the entire CAP trend (Fig. 1b). In the northeast United States and southeast Canada, increasing CAP intensity was also the dominant factor. Around Svalbard, however, CAP increases occurred both because of greater CAP intensity and greater frequency of CAP events (Fig. 1d).

Declines in CAP west of California in the Pacific Ocean and across Siberia are mostly caused by a decline in CAP frequency. In the Barents Sea, trends toward fewer events but higher intensity led to an insignificant trend in total CAP. Nowhere was a significant and robust trend in total CAP driven primarily by a change in CAP event duration.

Unlike in winter, summer CAP trends (Fig. 2a) have been more strongly controlled by CAP frequency, with declines in CAP frequency over eastern Europe and central Asia accounting for nearly all the declines in CAP, which exceed 15% (decade)$^{-1}$ in places (Figs. 2b,d). Pockets of increased CAP over the western Pacific and around Svalbard can similarly be linked primarily to increased CAP frequency. One minor exception to this pattern is northern Quebec, where

increased CAP is instead driven by slightly higher CAP intensity (Fig. 2c) and longer event duration (Fig. 2d). Summer exhibits less widespread significant trends in CAP intensity than winter, although the trends have also generally been positive (Fig. 2c).

b. Decomposition of CAP intensity trends

A common question asked in past studies regarding trends in precipitation is whether any given trend is driven by "thermodynamic" or "dynamic" changes (e.g., Cassano et al. 2007; Finnis et al. 2007; Yettella and Kay 2017). For example, a trend in CAP intensity may occur because of a change in cyclone intensity (a dynamic change) or moisture availability (a thermodynamic change). Using the decomposition outlined in section 3d, we find that the increases in winter CAP intensity observed over eastern North America, the Mediterranean, and the west side of the North Pacific and North Atlantic storm tracks have occurred because of both thermodynamic and dynamic changes (Fig. 3). In other words, more moisture is available, and wind speed in extratropical

a. CAP Change
(% per decade)

b. Regional Averages

c. CAP Change from
CAP Intensity

d. CAP Change from
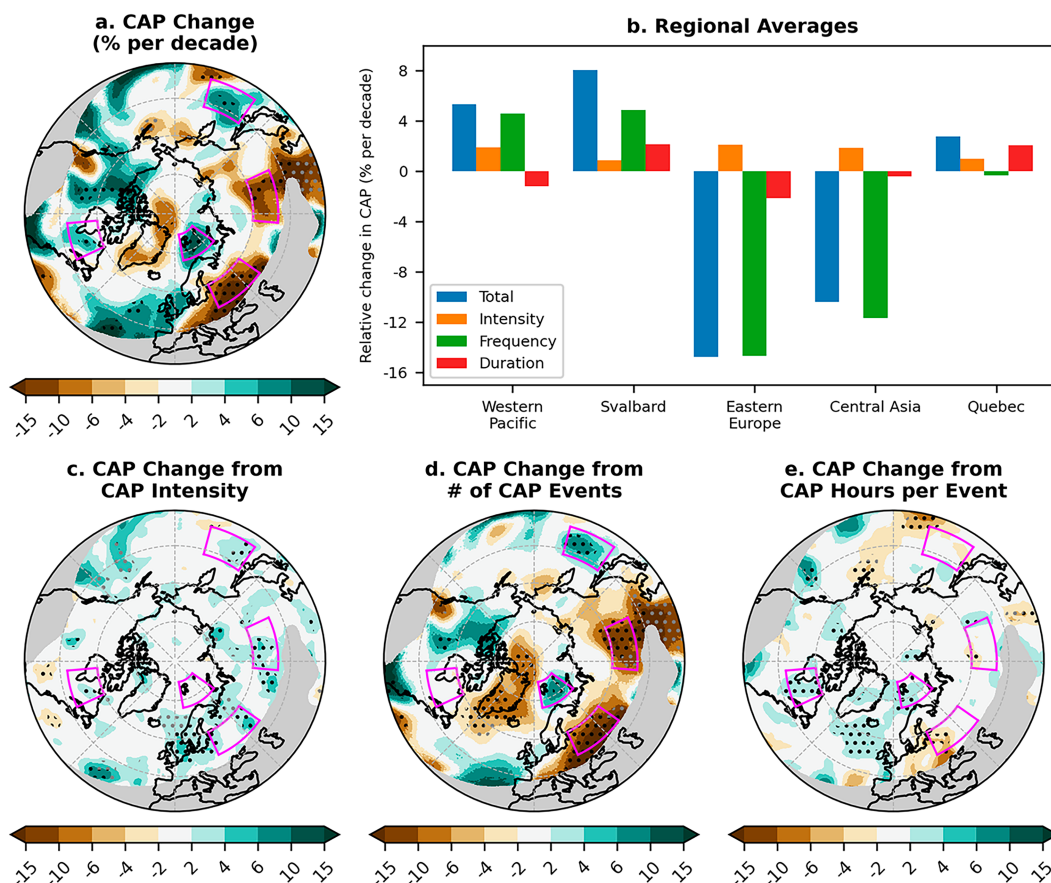# of CAP Events

e. CAP Change from
CAP Hours per Event

FIG. 2. As in Fig. 1, but for summer (JJA).

cyclones has strengthened. Over the Sea of Okhotsk, by contrast, greater CAP intensity is driven entirely by an increase in cyclone intensity.

Over the Arctic Ocean, increased CAP intensity in ERA5 is due exclusively to enhanced moisture availability. In fact, the trends in dynamics, if anything, would suggest a decline in CAP intensity. However, the results for the Arctic Ocean are uncertain since MERRA-2 and ERA5 do not agree on the trends (indicated by the gray stippling). Earlier results (Fig. 1c) showed better agreement, which may be because they were showing CAP related to myriad cyclone subfeatures, whereas the decomposition method used for cyclone intensity can only be applied to precipitation falling around the cyclone core. This omits some frontal precipitation and effectively smooths the precipitation fields.

Trends in summer CAP intensity have been less intense, with nowhere experiencing trends exceeding +4% (decade)$^{-1}$ (Fig. 4). The one area with significantly increasing CAP intensity is the Icelandic low region, where both thermodynamic and dynamic changes have contributed to the increase.

c. Decomposition of trends in CAP hours

The number of hours a location experiences CAP ("CAP hours") may change for a variety of reasons, which we organize into two main factors (section 3e). These are the number of hours an extratropical cyclone is over a location (cyclone hours) and the fraction of cyclone hours that also include CAP (CAP probability). In winter, significant trends in CAP hours are sparse, but generally, wherever a significant trend has occurred, it has been primarily because of a trend in CAP probability (Fig. 5). For example, the Barents Sea has experienced a slight decline in cyclone hours (which is insignificant) but a much larger (and significant) trend in CAP probability. Similarly, a roughly 4% (decade)$^{-1}$ increase in CAP hours over the central Arctic Ocean corresponds to both an increase in cyclone hours and CAP probability, but the contribution from CAP probability is about twice as large.

In summer, the relative change in CAP hours is stronger in many places, with declines exceeding 20% (decade)$^{-1}$ in eastern Europe and western Russia (Fig. 6). In this case, declines in cyclone hours and CAP probability are roughly equal in contribution but only total about a 10% (decade)$^{-1}$ drop in CAP hours, indicating some residual error in the decomposition. Increased CAP hours over Canada's Northwest Territories and the eastern Atlantic are explained by an increase in both cyclone hours and CAP probability, but as in winter, the latter factor is dominant. In other words, although trends in cyclone hours can partially explain some trends in CAP hours, trends in CAP probability are the more important factor. This
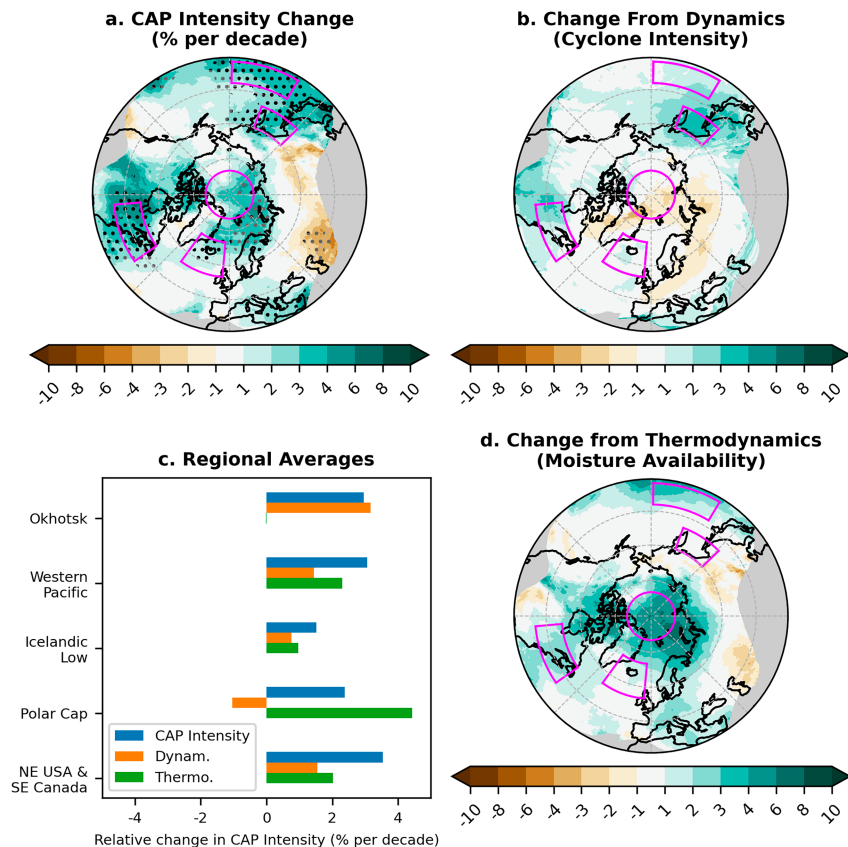
FIG. 3. (a) Relative change in CAP intensity $[\% \ (\text{decade})^{-1}]$ during winter (DJF) based on ERA5 (1979–2021), and decomposition of that response into two factors: (b) change from dynamics (measured as the relative frequency of discrete bins in the probability density function of 850-hPa average wind speed) and (d) change from thermodynamics (measured as the CAP intensity for each discrete wind speed bin). All units are percent change in CAP intensity per decade. Stippling in (a) indicates a significant trend ($p < 0.05$), with black (gray) stipples showing where MERRA-2 trends have the same (opposite) sign. (c) Regional averages of relative trend and its components for five illustrative areas (outlined in magenta in maps).

is notable since CAP probability may reflect both dynamic and thermodynamic drivers. For example, greater storm size and intensity can increase the chances that a cyclone produces CAP at a grid cell, but greater moisture availability could, too. Considered in conjunction with the previous section, this suggests a stronger role for thermodynamic factors in driving historical CAP trends.

5. CAP response to future warming

a. Overall trends in CAP

Using the multimodel mean of 18 CMIP6 models, positive trends in winter CAP are projected to be nearly ubiquitous throughout the Northern Hemisphere (Fig. 7a). The key exceptions are the Icelandic low, part of the Mediterranean, and around 30°–35°N in the Pacific Ocean. The Arctic and eastern Asia exhibit the strongest trends, with an over 30% increase in CAP (above the 1979–2014 average) per degree Celsius of global warming. As with historical trends, the increase in

CAP comes largely from increased CAP intensity (e.g., the Bering Sea and Atlantic Canada; Fig. 7c). However, in the areas of greatest increase in total CAP (the Arctic Ocean and northeast Asia), increased CAP frequency is the more dominant factor (Figs. 7b,d). Throughout both the Atlantic and Pacific Oceans, CAP frequency declines minorly (accounting for −2% to −5% CAP °C^{-1}), countering the increase in CAP intensity.

Like historical trends, event duration contributes minorly to projected CAP trends (Fig. 7e). Unlike historical trends, though, significant trends are positive throughout the Northern Hemisphere.

Continuing historical trends, summer CAP decreases with further warming over midlatitude Eurasia (Fig. 8a). In the future, declines in CAP are projected south of 60°N everywhere except the Pacific Ocean, which exhibits increased CAP. Increased CAP is also projected for the Arctic Ocean, Greenland, and Alaska. Note, though, that relative increases are much weaker for the Arctic Ocean
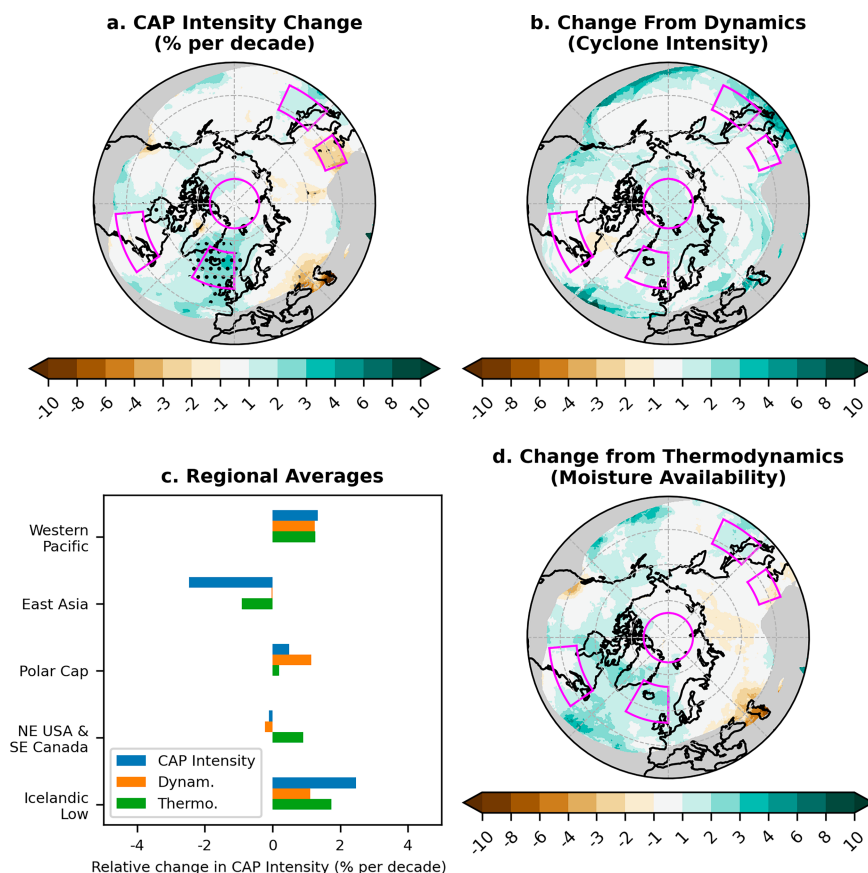
FIG. 4. As in Fig. 3, but for summer (JJA).

in summer than in winter (10%–15% CAP $°C^{-1}$ instead of >30% CAP $°C^{-1}$).

In general, greater CAP intensity encourages increased CAP throughout the Northern Hemisphere (Fig. 8c), but CAP frequency declines nearly everywhere south of 60°N (Fig. 8d). Only over the Pacific Ocean are increases from CAP intensity able to overcome declines in CAP frequency (Fig. 8b). The only area with increased CAP frequency spans Greenland and the central Arctic Ocean, which also experiences longer event duration; combined, these explain why this area exhibits the strongest CAP increases in summer.

b. Decomposition of future CAP intensity trends

CMIP6 models project that positive trends in CAP intensity will be dominated by moisture availability (Fig. 9). This tendency is most apparent for the Arctic Ocean, where models show a continuation of historical trends: slight weakening of cyclone wind speeds will contribute negatively to CAP intensity by 1%–2% $°C^{-1}$, but increased moisture availability will contribute positively to CAP intensity by about 20% $°C^{-1}$. Projections for summer similarly show moisture availability as dominant, both over the oceans and eastern Asia, where CAP intensity is projected to increase, and over southern Europe, where CAP intensity is projected to decrease (Fig. 10).

c. Decomposition of future trends in total CAP hours

The decomposition of historical trends in total CAP hours revealed greater contributions from trends in CAP probability and smaller contributions from trends in cyclone hours (Fig. 5). Projections from CMIP6 show that this pattern persists with continued warming for the Arctic in both seasons and for midlatitude continents in summer (Figs. 11 and 12). However, other projections differ from historical trends. For example, the projected decline in winter CAP hours over Japan is almost exclusively from a decline in cyclone hours, and declines in winter CAP hours over southern Europe are driven by declines in both factors (Fig. 11).

The much stronger relative increases in CAP hours over the Arctic Ocean, Arctic Canada, and eastern Siberia, which exceed 30% $°C^{-1}$, are driven almost entirely by increased CAP probability. In fact, throughout much of this region, the number of cyclone hours actually declines with further warming. Combined with the primacy of increased moisture availability in driving positive trends in CAP intensity in these same regions, these results demonstrate dominance by thermodynamic factors and minimal impact from dynamic factors in driving trends in CAP over the Arctic.

In summer (Fig. 12), projected declines in the number of CAP hours over the continents are caused jointly by declines in cyclone hours and in the CAP probability, although the
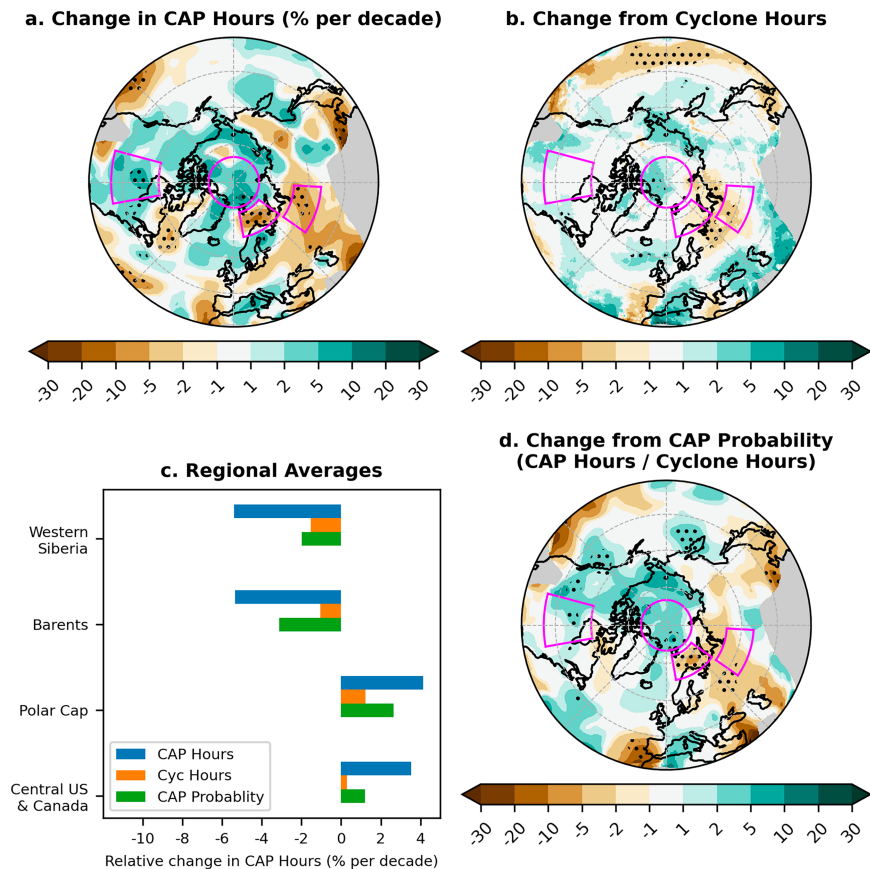
FIG. 5. (a) Relative change in the number of hours per winter (DJF) with nonzero CAP [% (decade)$^{-1}$] based on ERA5 (1979–2021), and decomposition of that response into two factors: (b) change from cyclone frequency (hours per winter for which a cyclone is present) and (d) change from the probability that a cyclone-influenced location experiences precipitation (i.e., the ratio of CAP hours to cyclone hours). All units are percent change in CAP hours per decade. Stippling indicates a significant trend ($p < 0.05$), with black (gray) stipples showing where MERRA-2 trends have the same (opposite) sign. (c) Regional averages of relative trend and its components for four illustrative areas (outlined in magenta in maps).

latter is typically the larger factor. Over the North Pacific Ocean, CAP probability increases, but the decline in cyclone hours more than compensates. As a result, CAP hours decline overall over the North Pacific, but not as dramatically as over other midlatitude regions. The Arctic Ocean and Greenland are the only places that experience increased CAP hours in summer, and this is driven exclusively by the increased probability of CAP during cyclone activity. Summer cyclone hours exhibit no clear trend over the central Arctic Ocean and slight declines along the Arctic periphery. Again, trends from thermodynamic factors prove dominant at high latitudes.

6. Discussion

This study used the historical and high-emission scenario SSP5–8.5 to assess how CAP responds to global warming for a range of annual global mean surface air temperature anomalies of roughly 0.5°–6.0°C (relative to 1850–1900). Cyclone responses to global warming are reliably linear (Crawford

et al. 2023), but precipitation responses are not (Liu and Allan 2013); therefore, it is important to recognize that the CAP trends reported are averages for that temperature range and not necessarily constant for each successive degree of warming. In addition to that caveat, several study limitations must be considered (section 6a) before discussing two key aspects of our results in the context of the broader literature: First, that trends in both frequency and intensity of CAP events dictate overall change (section 6b); and second, that the thermodynamic contribution dominates projected CAP trends (section 6c).

a. Study limitations

One complication of any CAP study is how to best associate precipitation with cyclones. Precipitation can be assigned based on a standard radius from a cyclone center (e.g., Utsumi et al. 2017; Oh et al. 2020) or based on the intersection of cyclone areas and precipitation areas (e.g., Finnis et al. 2007; Crawford and Serreze 2017). Precipitation can also be assigned to cold air outbreaks, fronts, and moisture transport
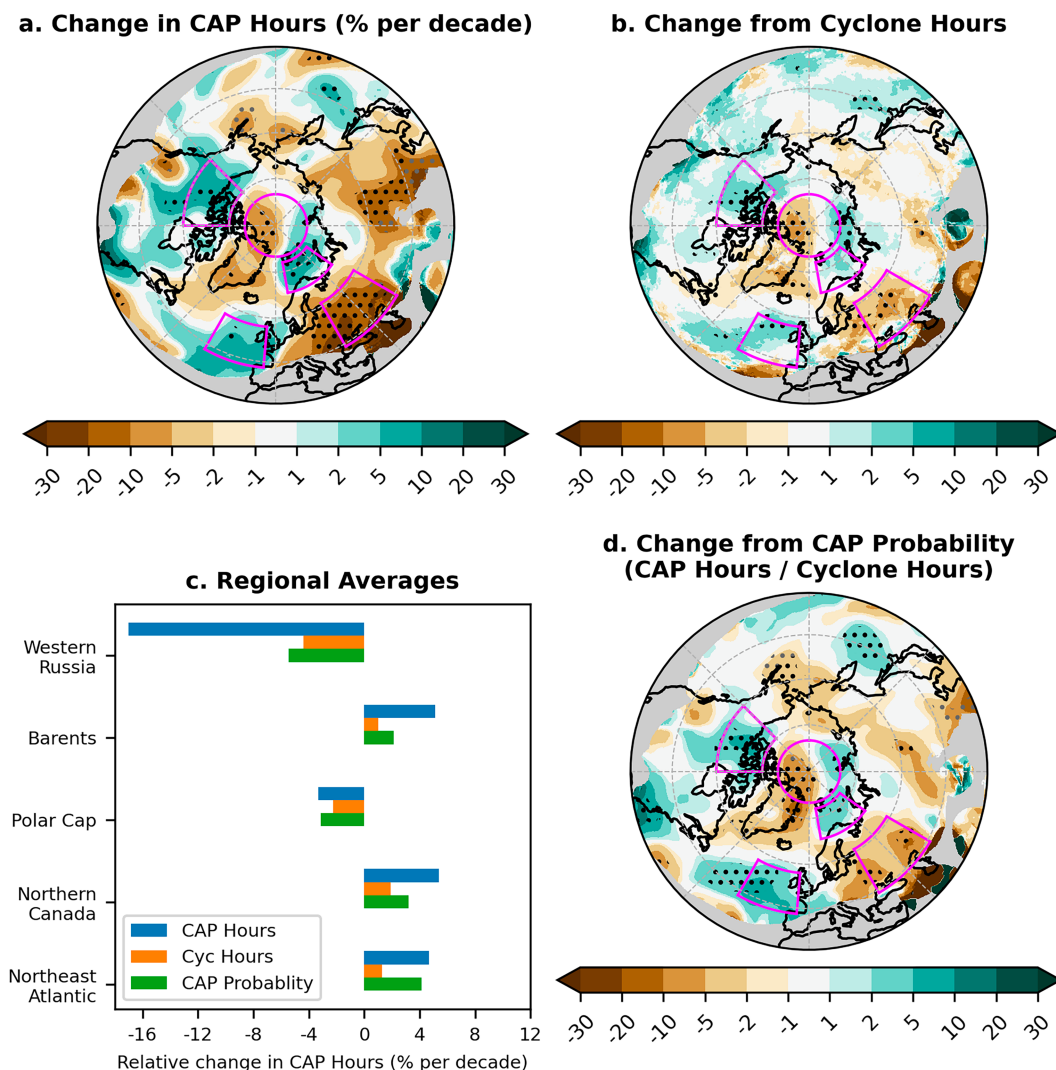
FIG. 6. As in Fig. 5, but for summer (JJA).

corridors, which are often, though not necessarily, a part of a larger extratropical cyclonic system (Rüdisühli et al. 2020; Konstali et al. 2024). For the main analysis here, we use the intersection of cyclone areas and precipitation areas for our assignment, providing an all-encompassing measure of CAP that can include precipitation far away from the cyclone center, such as along a lengthy front.

However, to decompose cyclone intensity into thermodynamic and dynamic components, we focus on the core cyclonic precipitation. This is both to allow better comparison to past literature and to focus on the core cyclonic precipitation likely to be most impacted by cyclone intensity, but it cannot fully capture the causes of trends in CAP intensity, especially frontal precipitation. Additionally, because the precipitation and wind are assigned to a single point, this process effectively applies a 1200-km smoother to the data, reducing the precision. This is most noticeable for ERA5 data, which has the highest initial spatial resolution (Fig. S1). These simplifications yield larger residuals for this analysis (Figs. 3b and 4b),

and higher confidence can be placed wherever we are able to use the more comprehensive and precise CAP calculation (Figs. 1, 2, 5–8, 11, and 12).

For the primary CAP detection method, we use large-scale precipitation to define the precipitation area boundaries, but we use total precipitation within those boundaries for CAP. Therefore, CAP includes both stratiform precipitation from the large-scale precipitation schemes and convective precipitation from mesoscale features. However, coarse spatial resolution limits the ability of these datasets to simulate mesoscale precipitation features, so it is worth considering (i) how consistent ERA5 results are with other datasets and (ii) how well CMIP6 models (which are even coarser spatial resolution) reproduce observed patterns. Most significant trends in ERA5 are consistent with the trends in MERRA-2 (Figs. S2–S7), especially in winter and especially for CAP frequency and duration (Figs. 1 and 2). CAP intensity trends show less agreement between reanalyses, especially when only core cyclone precipitation is considered (Figs. 1–4).
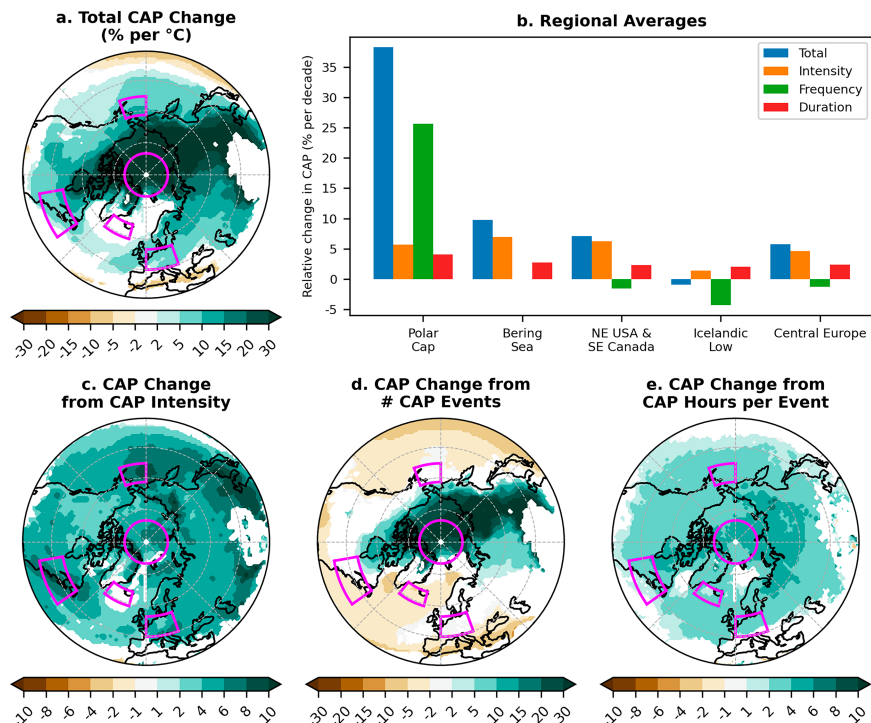
FIG. 7. (a) Relative change in total CAP (%) during winter (DJF) per degree Celsius of global warming, derived from the multimodel of 18 CMIP6 models (1979–2099), and decomposition of that response into four factors: (c) rate of precipitation during CAP events, (d) frequency of CAP events, and (e) average event duration. All units are percent change in CAP per degree Celsius. Areas where not all models agree on the sign of the response are masked. (b) Regional averages of relative trend and its components for four illustrative areas (outlined in magenta in maps).

Given the notable difference in spatiotemporal resolution, CMIP6 models produce remarkably similar CAP to ERA5 and MERRA-2 (Figs. S8 and S9), although that likely comes from compensating biases of CAP intensity being too weak and average CAP duration being too long. CMIP6 precipitation data have a coarser temporal resolution than the reanalysis data (6 hourly or daily instead of hourly), so short-duration, high-intensity precipitation events are effectively smoothed out, appearing as longer duration and lower intensity. After controlling for the bias in overall CAP intensity, the relative average CAP rate for each wind bin in the cyclone intensity decomposition is also very similar between the reanalyses and CMIP6 (Figs. S10 and S11).

Finally, we note that low-level wind speed is influenced by surface friction, so continental cyclones will average lower wind speeds than their marine counterparts. However, the number and width of the wind bins are sufficient to have an adequate distribution of cyclones for both continental and marine cases (Figs. S10 and S11); moreover, results of the intensity decomposition do not show a notable sensitivity to the choice of intensity metric (Figs. S12 and S13).

b. Trends in both frequency and intensity of CAP events dictate overall change

Continued warming is projected to increase CAP intensity in both seasons throughout nearly the entire mid- and high-

latitude Northern Hemisphere, leading to relative increases of over 6% CAP $°C^{-1}$ in eastern North America, East Asia, the North Pacific Ocean, and parts of the Arctic in winter (Fig. 7). This trend is consistent with both emerging trends from the reanalyses (though historical trends are less widespread; Fig. 1) and past studies (Yettella and Kay 2017; Akinsanola et al. 2020; Dou et al. 2022).

Future increased CAP intensity is combined with positive trends in CAP event frequency over Asia, the Arctic Ocean, and parts of Canada, leading to total CAP changes that exceed 30% $°C^{-1}$. Smaller magnitude decreases in CAP event frequency over the oceans and the Mediterranean partially counteract the intensity trend. The total CAP trend spatial pattern is like that described by Oh et al. (2020) for CMIP5 and GEMCLIM_Can: The Arctic shows the strongest relative change, and the Pacific Ocean shows more positive trends than the Atlantic Ocean.

Altogether, CAP frequency is the dominant factor driving CAP trends over the Arctic and Asia in winter, whereas intensity and frequency are equally important over other midlatitude regions. Finnis et al. (2007) found a similar balance between declining CAP frequency and increasing CAP intensity for the midlatitude oceans, but their Arctic results disagree with ours. For high latitudes, their decomposition showed a stronger influence from mean event output than event frequency under twenty-first-century warming using version 3
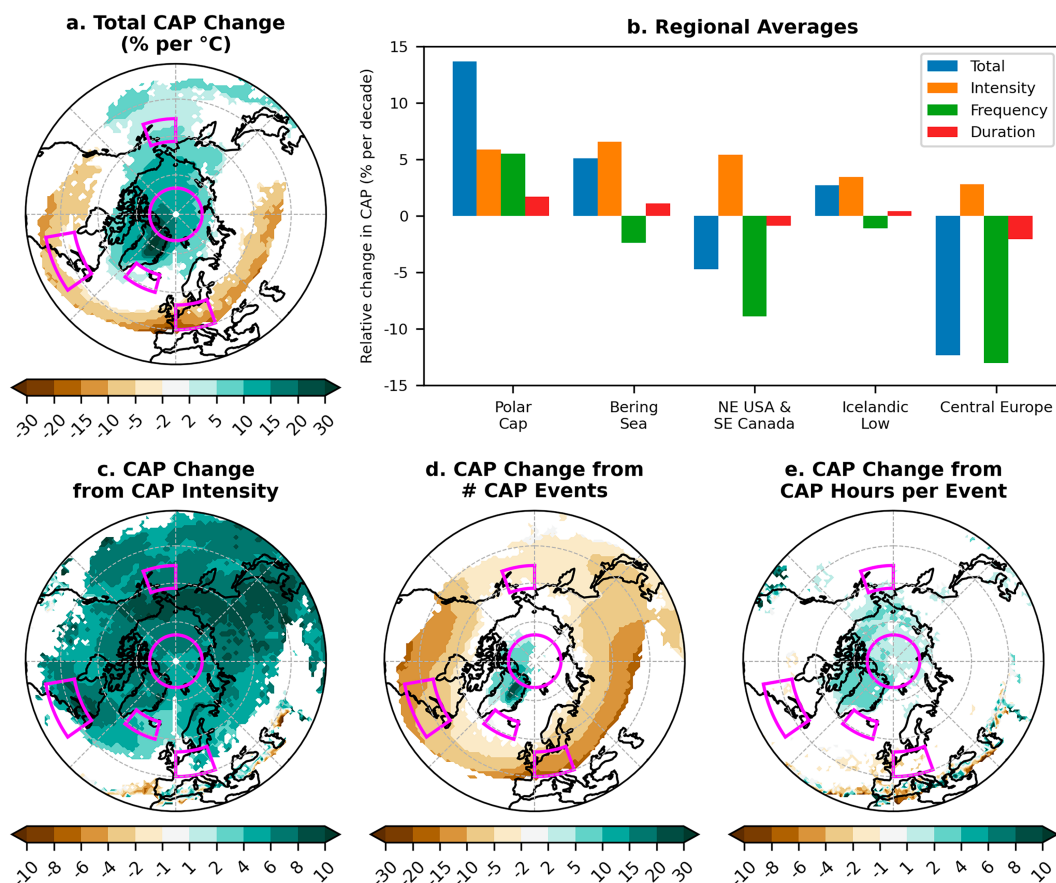
FIG. 8. As in Fig. 7, but for summer (JJA).

of the Community Climate System Model. The Arctic contains the lowest average CAP rates—near the 1.5 mm day^{-1} threshold for inclusion. Therefore, the number of CAP events may be sensitive to slight changes in precipitation rate, making discrepancies between different climate models more likely in the Arctic than in other regions.

CAP intensity also increases in summer throughout nearly the entire Northern Hemisphere, with the magnitude of impact on total CAP similar to winter. However, CAP event frequency exhibits substantial declines across a much wider swath of the midlatitudes, especially on the southern fringes of the continents (Fig. 7). In reanalyses, an historical decline in CAP frequency is apparent for Eurasia, although not North America (Fig. 2). As for winter, the reanalyses exhibit widespread positive trends for CAP intensity with few significant negative trends, but the positive trends are not ubiquitous as in CMIP6. This may reflect some bias in the models (see section 6a). It may also mean that internal variability is still strong enough to obscure the forced signal in some places.

The spatial pattern of summer CAP increases over the Arctic and Pacific Ocean and declines over the midlatitude continents, and Atlantic Ocean shown here is very similar to the CEMCLIM_Can results reported by Oh et al. (2020). Additionally, the CMIP6 multimodel mean appears to be in better agreement with their downscaled model than with their undownscaled CMIP5 results. Since CMIP6 models have demonstrated an overall improved ability to simulate synoptic-scale cyclone activity in the Northern Hemisphere compared to CMIP5 (Harvey et al. 2020), this is not surprising.

c. Thermodynamic contribution dominates projected CAP trends

Besides the balance of intensity versus frequency of events, another consideration is whether changes to CAP are primarily thermodynamic (related to the Clausius–Clapeyron relationship) or dynamic (related to changes in circulation, and to cyclone frequency and intensity). Some past work has emphasized thermodynamic factors, especially for CAP in the Arctic (Cassano et al. 2007; Crawford and Serreze 2017; Yettella and Kay 2017), but others have emphasized dynamic factors, especially cyclone intensity, when describing historical and future CAP trends (Stroeve et al. 2011; Oh et al. 2020).

Our CMIP6 results show dominance by thermodynamic factors. For CAP intensity, we follow the method of Yettella and Kay (2017). Our study agrees with theirs that thermodynamic contributions are dominant, but the dominance we find is even more consistent across space and season (Figs. 9 and 10). However, although historical trends suggest that thermodynamics dominate CAP intensity trends in the Arctic in winter,
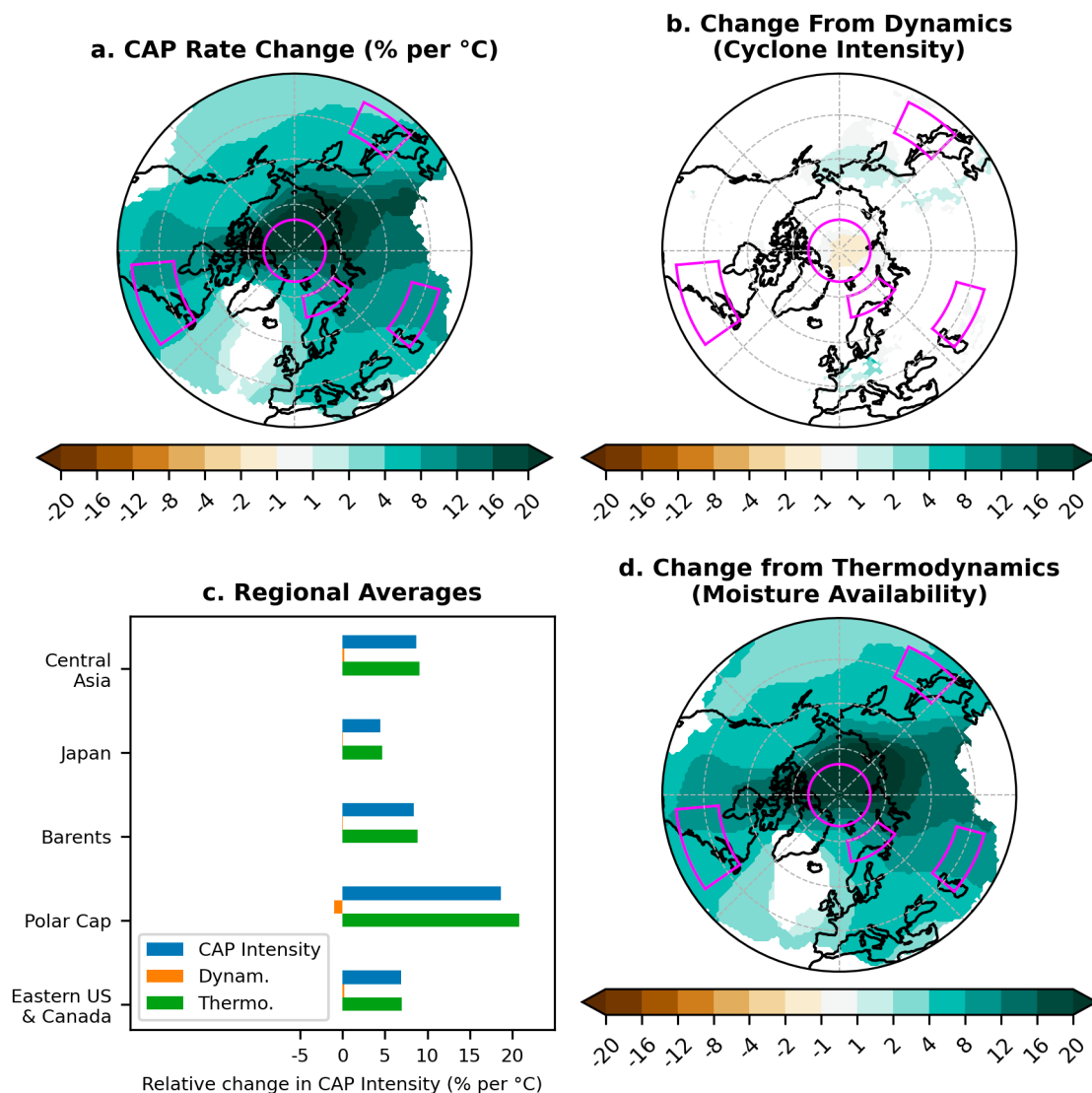
FIG. 9. (a) Relative change in CAP intensity (%) during winter (DJF) per degree Celsius of global warming, derived from the multimodel mean of 18 CMIP6 models (1979–2099), and decomposition of that response into two factors: (b) change from dynamics (measured as the relative frequency of discrete bins in the probability density function of 850-hPa average wind speed) and (d) change from thermodynamics (measured as the CAP intensity for each discrete wind speed bin). All units are percent change in CAP intensity per degree Celsius. Areas where not all models agree on the sign of the response are masked. (c) Regional averages of relative trend and its components for five illustrative areas (outlined in magenta).

historical dynamic contributions match or exceed thermodynamic contributions on the western end of the North Pacific and North Atlantic storm tracks in winter, and in several regions in summer (Figs. 3 and 4). The degree to which this represents internal variability in circulation (driving short-term trends) or model bias (leading to underemphasis of dynamic contributions in projections) is unclear. Comparing historical simulations of single-model large ensembles to the reanalysis results in a future study could help clarify this point.

CAP frequency trends may also arise from thermodynamic or dynamic factors, although the decomposition is less straightforward. Therefore, we could only decompose the trend in

CAP hours into a trend in cyclone hours and a trend in CAP probability (the ratio of CAP hours to cyclone hours). A decline in cyclone hours throughout most of the midlatitudes (especially in summer) is consistent with projections of declining cyclone frequency (Eichler et al. 2013; Priestley and Catto 2022; Crawford et al. 2023). However, in most areas, trends in CAP hours are not driven primarily by trends in the frequency or duration of cyclones, but rather the probability that cyclones, when present, will produce precipitation. The primacy of CAP probability trends driving the trends in CAP hours is most strongly observed in the Arctic in winter.
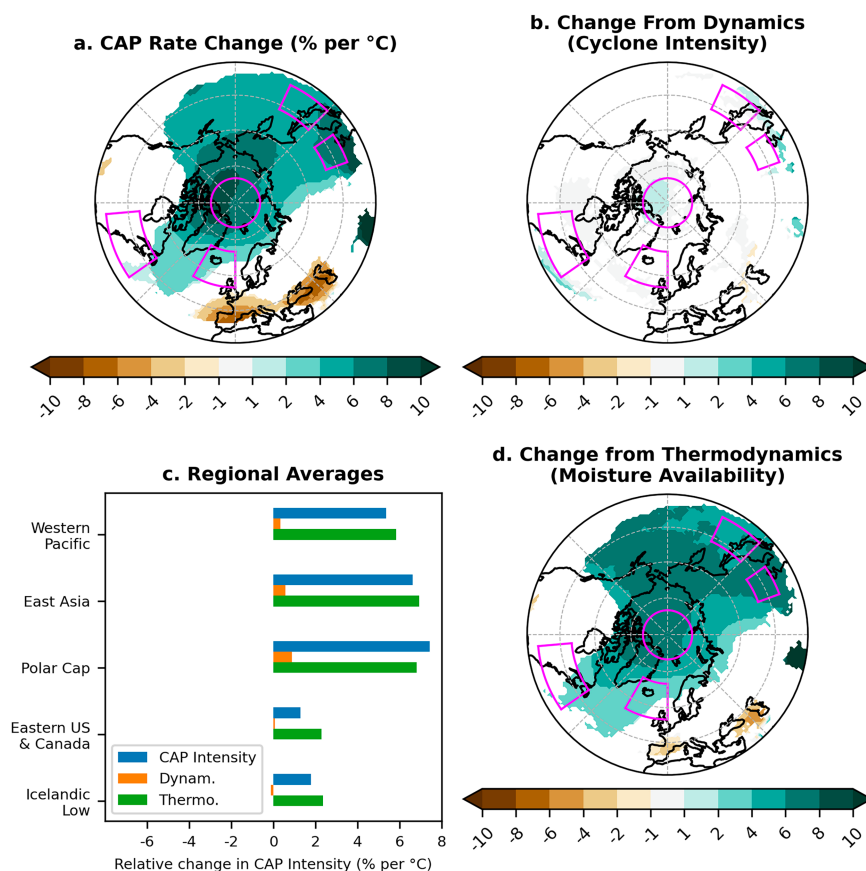
FIG. 10. As in Fig. 9, but for summer (JJA).

As with the decomposition of CAP intensity, though, we note that our CMIP6 results do not align with historical trends from reanalyses. Historical results are spatially patchy with many insignificant trends. When comparing to a multimodel mean, internal variability is undoubtedly a factor, but we cannot rule out model biases or other limitations as reasons for this difference. For example, CMIP6 models tend to simulate an excessively zonal North Atlantic storm track and underestimate summer cyclone activity over the Arctic Ocean (Harvey et al. 2020; Song et al. 2021; Priestley et al. 2023). Performance of individual CMIP6 models' simulation of precipitation compared to observational datasets varies greatly by region (Li et al. 2022) and may differ between annual precipitation, seasonal precipitation, and extremes (Agel and Barlow 2020). Few precipitation improvements have been reported compared to CMIP5 (Agel and Barlow 2020; J. Li et al. 2021; McCrystall et al. 2021), but at least in the Arctic, the multimodel mean annual precipitation in CMIP6 is a close match to ERA5 (McCrystall et al. 2021). Some studies have also noted greater ability to replicate observed cyclone or precipitation metrics by models with finer spatial resolution (e.g., Agel and Barlow 2020; Song et al. 2021; Crawford et al. 2023).

With these caveats in mind, the overall picture from the CMIP6 decompositions is that future trends in CAP are likely to be driven primarily by thermodynamic factors, especially in the high latitudes. Cyclone frequency trends are important, often amplifying or countering the dominant thermodynamic trend, but only in rare cases overwhelming it. This conclusion contrasts with Oh et al. (2020), whose data showed stronger correspondence between cyclone intensity trends and CAP trends. Oh et al. (2020) used an earlier version of the same cyclone and detection algorithm but different models and a different metric for cyclone intensity (central pressure vs wind speed). These differences may explain the discrepancy and our lack of evidence for meaningful cyclone intensity trends. That said, we also take additional steps to decompose the various drivers of CAP trends than previous studies, which allows us to better compare the relative importance of moisture availability versus dynamic drivers. Therefore, although we find a similar Atlantic–Pacific contrast in cyclone frequency trends as Oh et al. (2020), our results indicate that cyclone frequency is secondary to the increase in moisture availability in driving the trend in overall CAP.

7. Conclusions

With continued warming, CAP is projected to increase across the Northern Hemisphere in winter and over the Arctic Ocean and Pacific Ocean in summer. The strongest increases
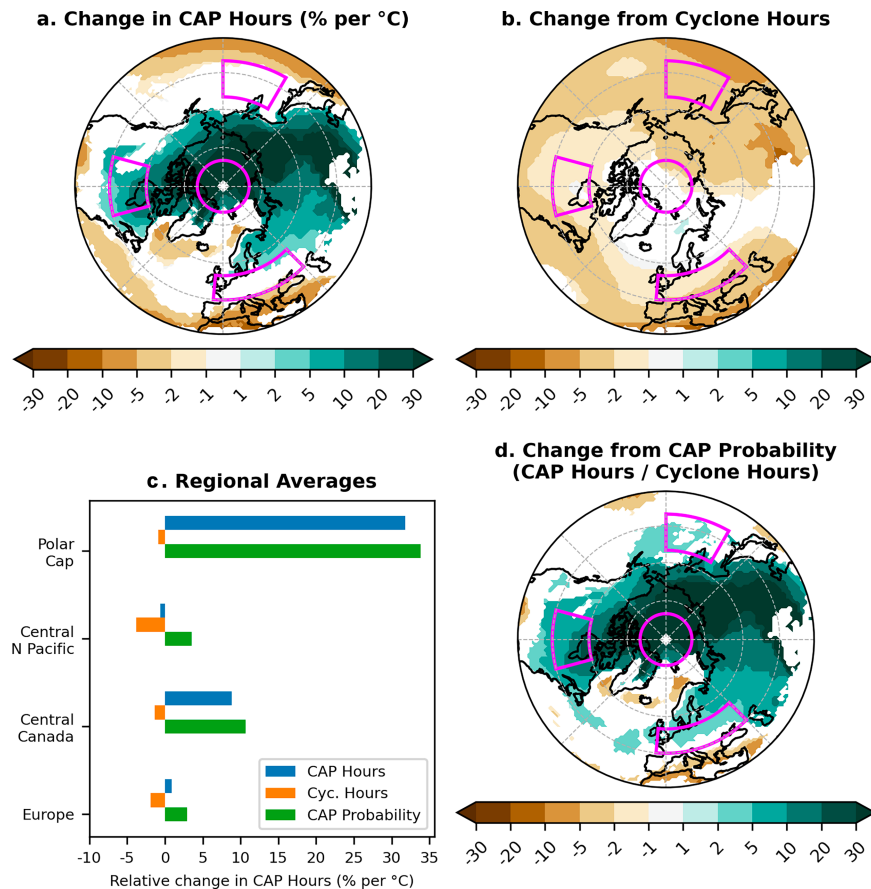
FIG. 11. (a) Relative change in CAP hours (%) during winter (DJF) per degree Celsius of global warming, derived from the multimodel mean of 18 CMIP6 models (1979–2099), and decomposition of that response into two factors: (b) change from cyclone frequency (measured as hours per winter for which a cyclone is present) and (d) change from the probability that a cyclone-influenced location experiences precipitation (i.e., the ratio of CAP hours to cyclone hours). All units are percent change in CAP hours per degree Celsius. Areas where not all models agree on the sign of the response are masked. (c) Regional averages of relative trend and its components for four illustrative areas (outlined in magenta in maps).

(over the Arctic Ocean) exceed 30% °C^{-1}. These increases are driven mostly by enhanced CAP intensity, although CAP also occurs more frequently over the Arctic Ocean in both seasons and over eastern Asia in summer. Conversely, CAP events become less frequent over the midlatitude oceans in both seasons and over the midlatitude continents in summer, which counteracts increasing CAP intensity and leads to an overall decline in CAP for the midlatitude continents and the Atlantic Ocean in summer. CAP events are projected to last longer in the future during winter throughout the Northern Hemisphere, and over the Arctic Ocean in summer.

Increasing CAP intensity in simulations of the future is predominantly controlled by increased moisture availability (a thermodynamic factor) rather than storm intensity (a dynamic factor). The changing number of CAP hours experienced by a location is also more commonly the result of trends in the probability of precipitation occurring when a cyclone is nearby rather than the number of hours with a cyclone present. The

dominance of thermodynamic factors is strongest in the Arctic, with dynamic factors (especially a decline in cyclone hours) being more relevant in the midlatitudes, though still rarely dominant.

The agreement between future projected trends and historical trends is mixed. For example, the decomposition of CAP intensity and CAP frequency trends yields spatially heterogeneous results with historical trends, especially in the midlatitudes. This is likely attributable in part to internal variability being averaged out in a multimodel ensemble mean but may also point to bias in the models. The more detailed decompositions have larger uncertainty than the overall CAP trend, but several general patterns found in the projections are already observable in the historical record:

1) Positive CAP trends are more common in winter than in summer.
2) The response of CAP to global warming generally depends on the balance between a decrease in CAP frequency (which
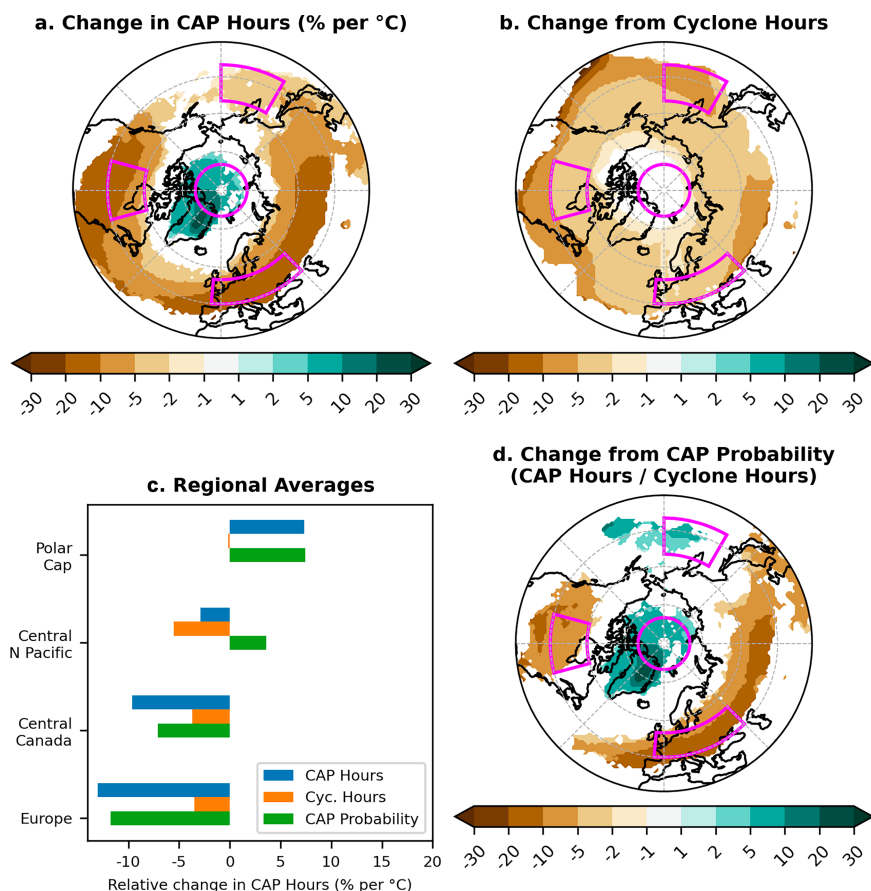
FIG. 12. As in Fig. 11, but for summer (JJA).

is in turn related to fewer cyclone hours) and an increase in the CAP intensity.

3) Finally, a decline in cyclone hours is more important to CAP in the midlatitudes, with the Arctic experiencing positive or neutral trends.

REFERENCES

Agel, L., and M. Barlow, 2020: How well do CMIP6 historical runs match observed Northeast U.S. precipitation and extreme precipitation–related circulation? *J. Climate*, **33**, 9835–9848, https://doi.org/10.1175/JCLI-D-19-1025.1.

Akinsanola, A. A., G. J. Kooperman, K. A. Reed, A. G. Pendergrass, and W. M. Hannah, 2020: Projected changes in seasonal precipitation extremes over the United States in CMIP6 simulations. *Environ. Res. Lett.*, **15**, 104078, https://doi.org/10.1088/1748-9326/abb397.

Allan, R. P., K. M. Willett, V. O. John, and T. Trent, 2022: Global changes in water vapor 1979–2020. *J. Geophys. Res. Atmos.*, **127**, e2022JD036728, https://doi.org/10.1029/2022JD036728.

Barrett, A. P., J. C. Stroeve, and M. C. Serreze, 2020: Arctic Ocean precipitation from atmospheric reanalyses and comparisons with North Pole drifting station records. *J. Geophys. Res. Oceans*, **125**, e2019JC015415, https://doi.org/10.1029/2019JC015415.

Bengtsson, L., K. I. Hodges, S. Koumoutsaris, M. Zahn, and N. Keenlyside, 2011: The changing atmospheric water cycle in Polar Regions in a warmer climate. *Tellus*, **63A**, 907–920, https://doi.org/10.3402/tellusa.v63i5.15872.

Cassano, J. J., P. Uotila, A. H. Lynch, and E. N. Cassano, 2007: Predicted changes in synoptic forcing of net precipitation in large Arctic river basins during the 21st century. *J. Geophys. Res.*, **112**, G04S49, https://doi.org/10.1029/2006JG000332.

Crawford, A. D., and M. C. Serreze, 2017: Projected changes in the Arctic frontal zone and summer Arctic cyclone activity in the CESM large ensemble. *J. Climate*, **30**, 9847–9869, https://doi.org/10.1175/JCLI-D-17-0296.1.

——, E. A. P. Schreiber, N. Sommer, M. C. Serreze, J. C. Stroeve, and D. G. Barber, 2021: Sensitivity of Northern Hemisphere cyclone detection and tracking results to fine spatial and temporal resolution using ERA5. *Mon. Wea. Rev.*, **149**, 2581–2598, https://doi.org/10.1175/MWR-D-20-0417.1.

——, J. V. Lukovich, M. R. McCrystall, J. C. Stroeve, and D. G. Barber, 2022: Reduced sea ice enhances intensification of winter storms over the Arctic Ocean. *J. Climate*, **35**, 3353–3370, https://doi.org/10.1175/JCLI-D-21-0747.1.

——, M. R. McCrystall, J. V. Lukovich, and J. C. Stroeve, 2023: The response of extratropical cyclone propagation in the Northern Hemisphere to global warming. *J. Climate*, **36**, 7123–7142, https://doi.org/10.1175/JCLI-D-23-0082.1.

Dou, T. F., S. F. Pan, R. Bintanja, and C. D. Xiao, 2022: More frequent, intense, and extensive rainfall events in a strongly warming Arctic. *Earth's Future*, **10**, e2021EF002378, https://doi.org/10.1029/2021ef002378.

Eichler, T. P., N. Gaggini, and Z. Pan, 2013: Impacts of global warming on Northern Hemisphere winter storm tracks in the CMIP5 model suite. *J. Geophys. Res. Atmos.*, **118**, 3919–3932, https://doi.org/10.1002/jgrd.50286.

Emori, S., and S. J. Brown, 2005: Dynamic and thermodynamic changes in mean and extreme precipitation under changed climate. *Geophys. Res. Lett.*, **32**, L17706, https://doi.org/10.1029/2005GL023272.

Fearon, M. G., J. D. Doyle, D. R. Ryglicki, P. M. Finocchio, and M. Sprenger, 2021: The role of cyclones in moisture transport into the Arctic. *Geophys. Res. Lett.*, **48**, e2020GL090353, https://doi.org/10.1029/2020GL090353.

Finnis, J., M. M. Holland, M. C. Serreze, and J. J. Cassano, 2007: Response of Northern Hemisphere extratropical cyclone activity and associated precipitation to climate change, as represented by the Community Climate System Model. *J. Geophys. Res.*, **112**, G04S42, https://doi.org/10.1029/2006JG000286.

Gelaro, R., and Coauthors, 2017: The Modern-Era Retrospective Analysis for Research and Applications, version 2 (MERRA-2). *J. Climate*, **30**, 5419–5454, https://doi.org/10.1175/JCLI-D-16-0758.1.

Harvey, B. J., P. Cook, L. C. Shaffrey, and R. Schiemann, 2020: The response of the Northern Hemisphere storm tracks and jet streams to climate change in the CMIP3, CMIP5, and CMIP6 climate models. *J. Geophys. Res. Atmos.*, **125**, e2020JD032701, https://doi.org/10.1029/2020JD032701.

Hawcroft, M. K., L. C. Shaffrey, K. I. Hodges, and H. F. Dacre, 2012: How much Northern Hemisphere precipitation is associated with extratropical cyclones? *Geophys. Res. Lett.*, **39**, L24809, https://doi.org/10.1029/2012GL053866.

Held, I. M., and B. J. Soden, 2006: Robust responses of the hydrological cycle to global warming. *J. Climate*, **19**, 5686–5699, https://doi.org/10.1175/JCLI3990.1.

Hersbach, H., and Coauthors, 2018: ERA5 hourly data on pressure levels from 1979 to present. Copernicus Climate Change Service (C3S) Climate Data Store (CDS), accessed 5 September 2023, https://doi.org/10.24381/cds.bd0915c6.

——, and Coauthors, 2020: The ERA5 global reanalysis. *Quart. J. Roy. Meteor. Soc.*, **146**, 1999–2049, https://doi.org/10.1002/qj.3803.

Hu, X., J. Shi, X. Ma, R. Ding, Z. Jing, and Y. Zhang, 2023: Distinct features of mid-winter North Pacific storm track suppression associated with central and eastern Pacific El Niños. *Atmos. Res.*, **289**, 106769, https://doi.org/10.1016/j.atmosres.2023.106769.

Konstali, K., C. Spensberger, T. Spengler, and A. Sorteberg, 2024: Global attribution of precipitation to weather features. *J. Climate*, **37**, 1181–1196, https://doi.org/10.1175/JCLI-D-23-0293.1.

Li, C., T. Zhao, C. Shi, and Z. Liu, 2021: Assessment of precipitation from the CRA40 dataset and new generation reanalysis datasets in the global domain. *Int. J. Climatol.*, **41**, 5243–5263, https://doi.org/10.1002/joc.7127.

Li, J., R. Huo, H. Chen, Y. Zhao, and T. Zhao, 2021: Comparative assessment and future prediction using CMIP6 and CMIP5 for annual precipitation and extreme precipitation simulation. *Front. Earth Sci.*, **9**, 687976, https://doi.org/10.3389/feart.2021.687976.

Li, Z., T. Liu, Y. Huang, J. Peng, and Y. Ling, 2022: Evaluation of the CMIP6 precipitation simulations over global land. *Earth's Future*, **10**, e2021EF002500, https://doi.org/10.1029/2021ef002500.

Liu, C., and R. P. Allan, 2013: Observed and simulated precipitation responses in wet and dry regions 1850–2100. *Environ. Res. Lett.*, **8**, 034002, https://doi.org/10.1088/1748-9326/8/3/034002.

Loeb, N. A., A. Crawford, J. C. Stroeve, and J. Hanesiak, 2022: Extreme precipitation in the eastern Canadian Arctic and Greenland: An evaluation of atmospheric reanalyses. *Front. Environ. Sci.*, **10**, 866929, https://doi.org/10.3389/fenvs.2022.866929.

Lorenz, D. J., E. T. DeWeaver, and D. J. Vimont, 2010: Evaporation change and global warming: The role of net radiation and relative humidity. *J. Geophys. Res.*, **115**, D20118, https://doi.org/10.1029/2010JD013949.

McCrystall, M. R., J. Stroeve, M. Serreze, B. C. Forbes, and J. A. Screen, 2021: New climate models reveal faster and larger increases in Arctic precipitation than previously projected. *Nat. Commun.*, **12**, 6765, https://doi.org/10.1038/s41467-021-27031-y.

Naakka, T., T. Nygård, T. Vihma, J. Sedlar, and R. Graversen, 2019: Atmospheric moisture transport between mid-latitudes and the Arctic: Regional, seasonal and vertical distributions. *Int. J. Climatol.*, **39**, 2862–2879, https://doi.org/10.1002/joc.5988.

O'Gorman, P. A., and C. J. Muller, 2010: How closely do changes in surface and column water vapor follow Clausius–Clapeyron scaling in climate change simulations? *Environ. Res. Lett.*, **5**, 025207, https://doi.org/10.1088/1748-9326/5/2/025207.

——, R. P. Allan, M. P. Byrne, and M. Previdi, 2012: Energetic constraints on precipitation under climate change. *Surv. Geophys.*, **33**, 585–608, https://doi.org/10.1007/s10712-011-9159-6.

Oh, S.-G., L. Sushama, and B. Teufel, 2020: Arctic precipitation and surface wind speed associated with cyclones in a changing climate. *Climate Dyn.*, **55**, 3067–3085, https://doi.org/10.1007/s00382-020-05425-w.

Papritz, L., F. Aemisegger, and H. Wernli, 2021: Sources and transport pathways of precipitating waters in cold-season deep North Atlantic cyclones. *J. Atmos. Sci.*, **78**, 3349–3368, https://doi.org/10.1175/JAS-D-21-0105.1.

Pendergrass, A. G., and D. L. Hartmann, 2014: The atmospheric energy constraint on global-mean precipitation change. *J. Climate*, **27**, 757–768, https://doi.org/10.1175/JCLI-D-13-00163.1.

Pithan, F., and T. Jung, 2021: Arctic amplification of precipitation changes—The energy hypothesis. *Geophys. Res. Lett.*, **48**, e2021GL094977, https://doi.org/10.1029/2021GL094977.

Priestley, M. D. K., and J. L. Catto, 2022: Future changes in the extratropical storm tracks and cyclone intensity, wind speed,

and structure. *Wea. Climate Dyn.*, **3**, 337–360, https://doi.org/10.5194/wcd-3-337-2022.

——, D. Ackerley, J. L. Catto, K. I. Hodges, R. E. McDonald, and R. W. Lee, 2020: An overview of the extratropical storm tracks in CMIP6 historical simulations. *J. Climate*, **33**, 6315–6343, https://doi.org/10.1175/JCLI-D-19-0928.1.

——, ——, ——, and ——, 2023: Drivers of biases in the CMIP6 extratropical storm tracks. Part I: Northern Hemisphere. *J. Climate*, **36**, 1451–1467, https://doi.org/10.1175/JCLI-D-20-0976.1.

Rawlins, M. A., and Coauthors, 2010: Analysis of the Arctic system for freshwater cycle intensification: Observations and expectations. *J. Climate*, **23**, 5715–5737, https://doi.org/10.1175/2010JCLI3421.1.

Rinke, A., and Coauthors, 2019: Trends of vertically integrated water vapor over the Arctic during 1979–2016: Consistent moistening all over? *J. Climate*, **32**, 6097–6116, https://doi.org/10.1175/JCLI-D-19-0092.1.

Rohrer, M., O. Martius, C. C. Raible, and S. Brönnimann, 2020: Sensitivity of blocks and cyclones in ERA5 to spatial resolution and definition. *Geophys. Res. Lett.*, **47**, e2019GL085582, https://doi.org/10.1029/2019GL085582.

Rüdisühli, S., M. Sprenger, D. Leutwyler, C. Schär, and H. Wernli, 2020: Attribution of precipitation to cyclones and fronts over Europe in a kilometer-scale regional climate simulation. *Wea. Climate Dyn.*, **1**, 675–699, https://doi.org/10.5194/wcd-1-675-2020.

Serreze, M. C., J. Voveris, A. P. Barrett, S. Fox, P. D. Blanken, and A. Crawford, 2022: Characteristics of extreme daily precipitation events over the Canadian Arctic. *Int. J. Climatol.*, **42**, 10 353–10 372, https://doi.org/10.1002/joc.7907.

Song, J.-N., G. Fu, Y. Xu, Z.-Y. Han, Q.-Z. Sun, and H. Wang, 2021: Assessment of the capability of CMIP6 global climate models to simulate Arctic cyclones. *Adv. Climate Change Res.*, **12**, 660–676, https://doi.org/10.1016/j.accre.2021.07.007.

Stroeve, J. C., M. C. Serreze, A. Barrett, and D. N. Kindig, 2011: Attribution of recent changes in autumn cyclone associated precipitation in the Arctic. *Tellus*, **63A**, 653–663, https://doi.org/10.1111/j.1600-0870.2011.00515.x.

Sun, W., Y. Liang, H. Bi, Y. Zhao, J. Meng, and J. Zhang, 2022: Insight on poleward moisture and energy transport into the Arctic from ERA5. *Atmosphere*, **13**, 616, https://doi.org/10.3390/atmos13040616.

Trenberth, K. E., A. Dai, R. M. Rasmussen, and D. B. Parsons, 2003: The changing character of precipitation. *Bull. Amer. Meteor. Soc.*, **84**, 1205–1218, https://doi.org/10.1175/BAMS-84-9-1205.

Utsumi, N., H. Kim, S. Kanae, and T. Oki, 2017: Relative contributions of weather systems to mean and extreme global precipitation. *J. Geophys. Res. Atmos.*, **122**, 152–167, https://doi.org/10.1002/2016JD025222.

Vessey, A. F., K. I. Hodges, L. C. Shaffrey, and J. J. Day, 2020: An inter-comparison of Arctic synoptic scale storms between four global reanalysis datasets. *Climate Dyn.*, **54**, 2777–2795, https://doi.org/10.1007/s00382-020-05142-4.

Villamil-Otero, G. A., J. Zhang, J. He, and X. Zhang, 2018: Role of extratropical cyclones in the recently observed increase in poleward moisture transport into the Arctic Ocean. *Adv. Atmos. Sci.*, **35**, 85–94, https://doi.org/10.1007/s00376-017-7116-0.

Wentz, F. J., L. Ricciardulli, K. Hilburn, and C. Mears, 2007: How much more rain will global warming bring? *Science*, **317**, 233–235, https://doi.org/10.1126/science.1140746.

Yettella, V., and J. E. Kay, 2017: How will precipitation change in extratropical cyclones as the planet warms? Insights from a large initial condition climate model ensemble. *Climate Dyn.*, **49**, 1765–1781, https://doi.org/10.1007/s00382-016-3410-2.